In-situ Neutron Reflectometry to Determine Ge Self-Diffusivities and Activation Energy of Diffusion in Amorphous $Ge_{0.8}Si_{0.2}$

Erwin Hüger[1,2*], *Jochen* Stahn[3], and *Harald* Schmidt[1,2]

[1]Clausthal Centre for Materials Technology, Clausthal University of Technology, D-38678 Clausthal-Zellerfeld, Germany
[2]Solid State Kinetics Group, Institute of Metallurgy, Clausthal University of Technology, D-38678 Clausthal-Zellerfeld, Germany
[3] Paul Scherrer Institut, 5232 Villigen PSI, Switzerland

Abstract. Amorphous Ge-Si solid solutions are an interesting class of materials from the fundamental as well as the technological point of view. Self-diffusion of the constituents is an important process because of the inherent metastability. While self-diffusion was already examined in crystalline Ge_xSi_{1-x} ($0 < x < 1$) this is not the case for the amorphous counterparts. This work reports on Ge self-diffusivities obtained from in-situ neutron reflectometry measurements during isothermal annealing of ion-beam sputter-deposited amorphous $Ge_{0.8}Si_{0.2}$ films. The diffusivities are modified peculiarly fast with annealing time by a maximum factor of two due to structural relaxation. The diffusivities in the relaxed state are lower (higher) than in amorphous germanium (silicon). They follow the Arrhenius law and show an activation energy of (2.06 ± 0.1) eV, which equals that of amorphous germanium, but differs from that of amorphous silicon. Thus, it is concluded that the diffusion mechanism of Ge in amorphous $Ge_{0.8}Si_{0.2}$ and Ge are similar, despite of the presence of dispersed 20 at.% of Si.

1 Introduction

Ge-Si alloys are considered to improve state-of-the-art electronic devices which are still based on silicon, and to add new possibilities of performance such as optics to integrated circuits [1]. The difference in bonding distance in germanium and silicon lattices causes strain and modifies the electronic band structure with increasing electron and hole mobility [1]. Miniaturization in electronic integrated circuits is still an ongoing demand [1]. Miniaturization is correlated to material confinement with development of quantum well states in the occupied and non-occupied electronic band structures [2]. In particular, Ge-Si nanostructures are considered to provide a new scientific field regarding materials properties [1]. Ge-Si spintronics and efficient light emission even with indirect band-gap materials [1] beneficial for opto-electronic integrated circuits are examples. Amorphous nanoscaled Ge-Si is of particular interest for solar cells whose optical band gaps matching the whole solar radiation spectrum [3-5]. This work contributes to the scientific examination of Ge-Si nanostructures by the measurement of self-diffusion in thin amorphous Ge-Si films with an innovative in-situ diffusion measurement methodology based on neutrons [6].

Self-diffusion is the thermally activated migration of atoms in solids [7,8]. It is a basic transport process, important for precipitation, grain growth, oxidation, joining processes and plastic deformation [7,8] as well as for the functionality of fuel cells and batteries [9-12].

Atomic diffusion was in the past routinely investigated by radiotracer diffusion studies [7,8,13] with the disadvantage of using radioactive tracers and doing depth profiling with mechanical sectioning and limited depth resolution [13]. A further disadvantage of the radiotracer method is the lack of measuring diffusion in-situ, i.e. during the heat treatment without cooling down the sample. This is also the case for using stable tracer isotopes and depth profiling with secondary ion mass spectrometry (SIMS) [14-27].

In-situ measurement of diffusivities has the advantage of a significant reduction of the experimental time, a reduction of error limits due to lack of heating/cooling steps, and an identification of time-dependent processes [6]. In order to carry out such measurements, non-destructive methodologies are necessary.

* Corresponding author: erwin.hueger@tu-clausthal.de

Neutron reflectometry (NR) [6,25,28-52] is such a non-destructive methodology, where the neutrons do not interact with electrons and possess therefore a high penetration depth in almost all materials. For example, the neutron beam transmission through a 1 cm thick silicon wafer, Al metal, or sapphire is 99.5 %, 99.1 %, or 97.4 %, respectively [53]. This ability of neutrons allows neutron beam investigations during device operation. A typical example is the monitoring of atomic diffusion in-situ or in-operando [6,40,42-44] and in real time [6,40,42-44,46-52] during furnace operation (sample heating).

Self-diffusion investigations on amorphous Ge-Si alloys where not published until now. This is mainly due to the metastable [54] or even unstable [55] state of the amorphous structure, as predicted for amorphous silicon [54,55]. There, diffusivity has to be determined on short lengths scales in order not to average over different transient metastable states and to avoid unwanted crystallization. NR experiments are capable to measure small diffusion lengths down to 1 nm [6,28,31,38] and, hence, in transient states [31]. This study reports on in-situ self-diffusion investigations on amorphous $Ge_{0.8}Si_{0.2}$ films. The second section gives a review on recent literature results on germanium, silicon, and Ge-Si alloys. The third section describes the experimental procedure. The fourth section presents and discuss the experimentally derived in-situ NR results. A comparison to published results obtained for pure amorphous germanium and silicon will be given. The results are summarized in the fifth section.

2 Literature survey on self-diffusion in Ge, Si and Ge-Si alloys

Ge-Si is a completely miscible system [1]. Thus, Ge-Si compounds with any Ge content can be produced [1]. There is a lack of reports on self-diffusion in amorphous Ge_xSi_{1-x}. However, this is not the case for crystalline Ge_xSi_{1-x}, where self-diffusion was examined by a few research groups [13,23-25,38]. In general, the Si and Ge self-diffusivities are similar due to the valence isoelectronicity of the two species, and they decrease with increasing Si content. Figure 1 gives an overview. The activation energy of self-diffusion of dependence on the Ge content in Ge_xSi_{1-x} with x between 0 and 1 is plotted. Results were reported for Ge_xSi_{1-x} single crystals in form of epitaxial films as obtained by Zangenberg et al. [23] (green circles), and more recently by Kube et al. [24] (red dots and blue squares), as well as for polycrystalline Ge_xSi_{1-x} [13] (black filled triangles).

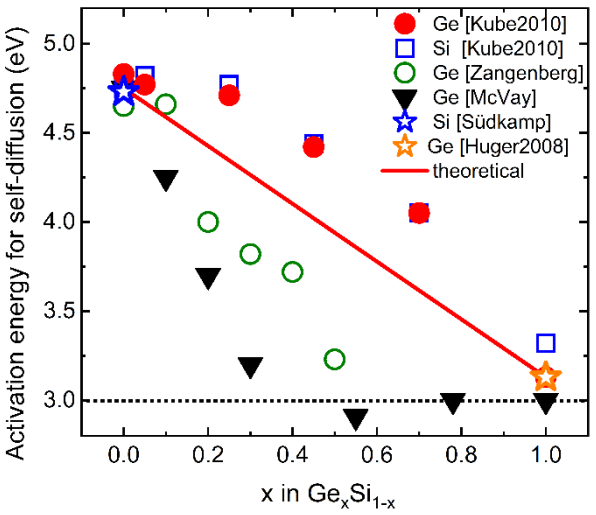

Fig. 1. Activation energy of self-diffusion in crystalline Ge_xSi_{1-x}. The references by Südkamp et al. [26] and Hüger et al. [38] provides values for Si self-diffusion for x = 0 (pure silicon) and for Ge self-diffusion for x = 1 (pure germanium) which are marked with a blue star and an orange star, respectively. The red dots and the blue squares mark the results by Kube et al. [24] for Ge and Si self-diffusion in epitaxial films. The green circles mark the results on Ge self-diffusion obtained by Zangernberg et al. [23], also on epitaxial films. The black filled triangles are for Ge self-diffusion in polycrystalline Ge_xSi_{1-x} obtained by McVay et al. [13]. The expected diffusivity behaviour according to equation (1) is marked with a red continuous line.

The activation energy of Ge self-diffusion is similar to that of Si self-diffusion for the same Ge content (results of Kube et al. [24]). The self-diffusivity examined in crystalline pure germanium can be accurately described over nine orders of magnitude by a single Arrhenius straight line [38]. A diffusion mechanism taking place by single-vacancies is postulated with an activation energy of (3.13 ± 0.03) eV for temperatures between 429 °C and 904 °C. Calculations [56] predict that the vacancy formation energy in crystalline germanium is positive and lower than in crystalline silicon. Consequently, vacancies in germanium are more prevalent than in silicon [56]. Thus, the situation for self-diffusion in crystalline pure silicon is more complicate [25,26], where contributions of self-interstitials and vacancies have to be considered. Self-diffusivities over ten orders of magnitude were determined from experiments [25]. An activation energy of self-diffusion of 4.73 eV is reported [26]. Hence, the examination of self-diffusion in Ge_xSi_{1-x} alloys is of interest also from the view point of fundamental diffusion science. It has to be clarified if a germanium-like diffusion mechanism or a silicon-like diffusion mechanism is operating predominantly in Ge_xSi_{1-x}.

For crystalline Ge_xSi_{1-x} alloys, the reported activation energy decreases with increasing Ge content x (Figure 1). As a simple approximation, the activation energy vs Ge content should obey to the Vegard's law [24]:

$$E_A(x) = (1-x)E_A^{Si} + xE_A^{Ge} \quad . \qquad (1)$$

This behaviour was clearly not observed in all the literature studies (Figure 1). The results of Kube et al. [24] show an enhancement and that of the other authors a reduction of the activation energies in comparison to the behaviour predicted by equation (1) (see the red continuous line in Figure 1). For example, the single-crystalline Ge_xSi_{1-x} epitaxial films with the relative high Ge composition of x = 0.7 gives [24] an activation energy of self-diffusion of 4.05 eV which is still more close to that of pure silicon (4.73 eV) than to that of pure germanium (3.13 eV). This indicates a diffusion behaviour similar to crystalline silicon. This is not the case for the activation energy of Ge self-diffusion in polycrystalline Ge_xSi_{1-x} (Figure 1) [13], which reaches that of pure Ge already for x = 0.3 and remains constant for higher Ge contents (Figure 1). All activation energies reported by McVay lie below the straight line corresponding to equation (1), which was attributed to self-diffusion via grain boundaries in the polycrystalline Ge_xSi_{1-x} structure. The results of Zangenberg et al. [23] are older compared to that of Kube et al. [24] but are also on epitaxial Ge_xSi_{1-x} films. Their results are more similar to that of McVay et al. [13].

Investigations on self-diffusion in amorphous Ge_xSi_{1-x} were not reported until now. However, reports exist for the edge systems pure amorphous germanium [6,40] and silicon [39,27]. Recent computer calculations [54,55,57] suggest, that although the local order of amorphous silicon is close to that of crystalline silicon, the energetics of defect formation [54,55] and the diffusion mechanism [57] strongly differ. The formation energy of point defects such as vacancies, self-interstitial and dangling bonds is negative [54,55]. This means that defect production is spontaneous and does not need thermal energy in the case of the amorphous state which is contrary to the situation in the crystalline state. The self-diffusion mechanism in amorphous silicon is predicted by calculations also to be different from that in crystalline material in a way that well-defined elemental jump lengths do not exist in the amorphous network [57]. The self-diffusion proceeds by atomic bond rearrangement [57]. Experimentally, the self-diffusivities in amorphous silicon were found [27,39] to be many orders of magnitude higher than in crystalline silicon [25]. It was suggested from experimental data that self-diffusion in amorphous silicon films is mediated by local bond rearrangement leading to an activation energy of (2.70 ± 0.10) eV [27] for samples amorphisized by ion implantation or, alternatively by the migration of extended point defects leading to an activation energy of (4.4 ± 0.3) eV for samples produced by sputter deposition [39].

The energetics of defects and the diffusion mechanism in amorphous germanium is expected to be roughly similar to that in amorphous silicon. For amorphous germanium (sputter deposition), NR experiments found that the self-diffusivities are many orders of magnitude larger than in crystalline germanium [6,40] due to a lower activation energy of (2.11 ± 0.12) eV instead of (3.13 ± 0.03) eV. This indicates different diffusion mechanisms in crystalline and amorphous modifications. Local bond rearrangement is also suggested here as diffusion mechanism [6]. Within this work, the Ge self-diffusion in amorphous $Ge_{0.8}Si_{0.2}$ films is investigated and the results are compared with literature.

3 Experimental procedure

The amorphous $Ge_{0.8}Si_{0.2}$ samples in form of thin films were prepared by reactive ion-beam co-sputter deposition. Segmented targets were used to tailor the requested composition. Figure 2a,b presents photographs of the segmented targets. The thin films are produced in form of isotope [$^{73}Ge_{0.8}Si_{0.2}$ (14 nm) / $^{nat}Ge_{0.8}Si_{0.2}$ (14 nm)] × 10 multilayers (MLs). The base of the method is given in references [6,28-30,38]. The natural isotope abundance of germanium, termed ^{nat}Ge, consists of ^{70}Ge (20.5%), ^{72}Ge (27.4%), ^{73}Ge (7.8%), ^{74}Ge (36.5%), and ^{76}Ge (7.8%). The germanium target termed ^{73}Ge possesses a 95% ^{73}Ge isotope enrichment. For sputter target production, 1 mm thick polycrystalline ^{nat}Ge and ^{73}Ge disks with 20 mm diameters (MaTeck GmbH, Jülich, Germany) were bonded on a copper target holder. On top of the Ge disks, a quadrant of a 1 mm thick polycrystalline Si disk of 20 mm diameter (MaTeck GmbH, Jülich, Germany) was bonded as it is visualized in Figure 2a,b, to produce segmented targets. There is a three times larger Ge surface than silicon surface.

The depositions were performed using a sputter coater (IBC 681, Gatan, USA), equipped with two Penning sources. Ar^+ ion beams (5 kV, 180 µA) were used for film deposition. The targets were used successively without breaking the vacuum with a base pressure below 5×10^{-7} mbar. During deposition, the specimen is rotated (30 rotations per minute) and rocked (rock angle: 30° and rock speed: 15° per second) to ensure well dispersed Ge and Si atoms in the deposited film. (100) oriented, polished, nominally undoped silicon wafers (CrysTec GmbH, Berlin, Germany) were used as substrates for the MLs. For Raman spectroscopy and for energy dispersive X-ray spectroscopy (EDX) examination, the films were deposited on (0001) oriented, polished, saphire wafers (CrysTec GmbH, Berlin, Germany) and on flat Cu foils, respectively. The substrates were cleaned with isopropanol beforehand. The as-deposited multilayers have an overall thickness of 280 nm. Additional annealing was not applied to the deposited amorphous layers in the sputter chamber before removal and handling in air. According to literature, the self-heating of the sample during ion-beam sputter experiments is generally low (below 80 °C) due to the low impact energy (tens of eV) of ions which are deposited [6]. The native oxide layer of the substrates was not removed.

The multilayers were examined exclusively with non-destructive measurement techniques. X-ray reflectometry (XRR) and grazing incidence X-ray diffraction (GI-XRD) was done ex-situ with a Bruker D8 DISCOVER (Germany) diffractometer ($Cu_{K\alpha}$, 40 keV, 40 mA). The GI-XRD measurements were performed with 1° incident angle. Raman scattering was performed also ex-situ on a Bruker SENTERRA Raman microscope with a laser of 532 nm wavelength. For

more information and references on Raman scattering, the reader is referred to a recent work [58]. EDX was performed ex-situ with a High-Resolution Scanning Electron Microscope (SEM, EVO 15, Zeiss). Except in-situ NR measurements, all other measurements were performed at room temperature.

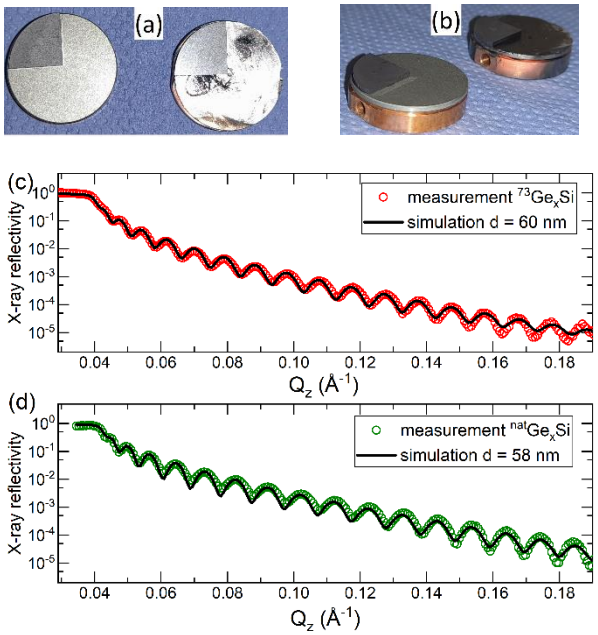

Fig. 2. a,b) top view (a) and side view (b) photographs of the segmented ^{nat}GeSi (left) sputter target and ^{73}GeSi (right) target to produce isotope ML. c,d) XRR data (circles) and corresponding simulations (Parratt32) for films deposited from the ^{73}GeSi or ^{nat}GeSi target.

NR was performed in-situ, meaning during isothermal heating of the ML sample inside a rapid thermal annealing oven (RTA AO500 MBE Komponenten, Germany) in argon gas. The NR examination was performed on the reflectometer AMOR at SINQ, Paul Scherrer Institut, Switzerland [42, 59]. The focusing Selene guide implemented there reduces the counting time considerably for small scattering vectors and specular measurements, only. Reflectometry simulations were performed using the Parratt32 software package [60].

The layer deposition rate was determined with the help of XRR measurements (Figure 2c and 2d). Thicknesses of (60 ±1) nm and (58 ±1) nm are obtained for as-deposited $^{73}Ge_xSi$ and $^{nat}Ge_xSi$ films (each 16 minutes of deposition time). Hence, the deposition rate from the $^{73}Ge_xSi$ and $^{nat}Ge_xSi$ target was (3.75 ± 0.06) nm and (3.62 ± 0.06) nm per minute, respectively, in good agreement.

4 Results and discussion

4.1 Sample characterization

EDX investigations found a relative amount of 80 at.% germanium and 20 at.% silicon (i.e., $Ge_{0.8}Si_{0.2}$) in films deposited from the $^{73}Ge_xSi$ and also the $^{nat}Ge_xSi$ target, indicating no or only minor chemical contrast within a bilayer

Figure 3 presents the measured GI-XRD data of the isotope $Ge_{0.8}Si_{0.2}$ ML (curves (a-c)) in comparison to that of isotope modulated pure Ge MLs (curves (d-f)). Both as-deposited materials are X-ray amorphous. The GI-XRD data show a lack of long-range order but the existence of local order (curves (a,d)). The heat treatment of the pure Ge ML at 418 °C for three hours and at 425 °C for one hour results in crystalline germanium (curves (e,f)). This is not the case for the amorphous $Ge_{0.8}Si_{0.2}$ ML (curves (b,c)) for even higher temperatures and longer annealing times. The XRD investigations clearly show that the presence of silicon inhibits the crystallization of the amorphous $Ge_{0.8}Si_{0.2}$ ML compared to Ge ML. Thus, the diffusion experiments performed in this work were done on X-ray amorphous $Ge_{0.8}Si_{0.2}$ layers.

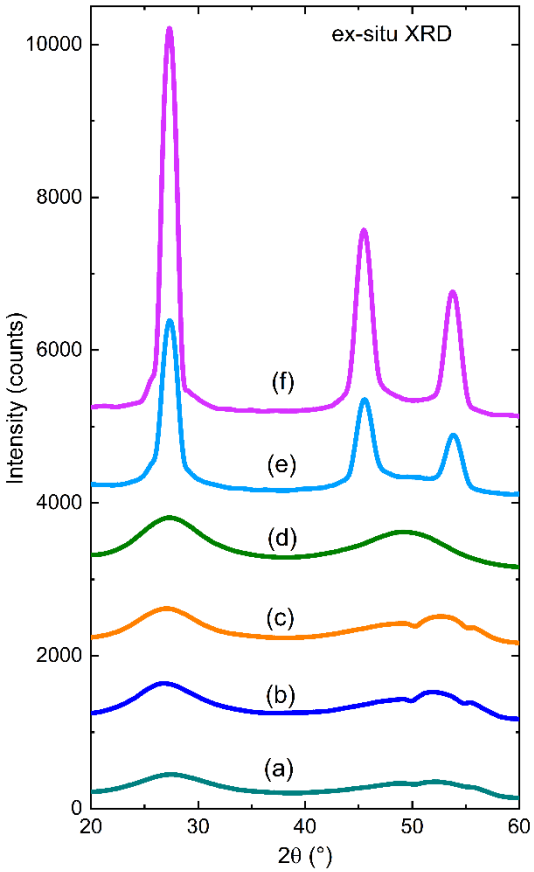

Fig. 3. GI-XRD data of the $Ge_{0.8}Si_{0.2}$ isotope ML (curves marked with (a-c)) compared to that of a pure Ge isotope ML film (curves marked with (d-f)). (a,d) As-deposited films. (b,c) After in-situ NR measurements of $Ge_{0.8}Si_{0.2}$ isotope MLs during isothermal annealing at 415 °C for 14 hours (curve (b)), and at 436 °C for 7 hours (curve (c)). (e,f) After in-situ NR measurements of pure Ge isotope MLs during isothermal annealing at 418 °C for 3 hours (curve (e)), and at 425 °C for 1 hour (curve (f)).

Figure 4 presents the Raman scattering measurements of the amorphous $Ge_{0.8}Si_{0.2}$ film (Figure 4b) in comparison to that of amorphous pure Ge film (Figure 4a) and additionally, an amorphous Si-rich $Ge_{0.25}Si_{0.75}$ film (Figure 4c). The amorphous $Ge_{0.25}Si_{0.75}$

film was obtained by using three instead of one quadrants of Si pieces for the sputter-target (see Figure 2a,b). The dashed vertical lines show the wave number position of Raman bands for amorphous germanium and amorphous silicon as found in literature [61-63]. Ge-Si local bonds produces Raman lines between the pure substances [61-63]. In the $Ge_{0.8}Si_{0.2}$ film (Figure 4b), there are no Si-Si bonds. The Si atoms are well dispersed into the amorphous germanium matrix. This slightly shifts the Raman emission of amorphous germanium to higher wave numbers (Figure 4b), as expected. In the case of the higher silicon content of the amorphous $Ge_{0.25}Si_{0.75}$ film (Figure 4c), there exist also Raman scattered intensity at the position of pure amorphous silicon. This means that for the $Ge_{0.25}Si_{0.75}$ film there exist Si atoms with only Si nearest neighbour atoms. Raman intensity is enhanced also between the peaks of the pure amorphous films without producing distinct peaks (Figure 4c). This means that the amorphous $Ge_{0.25}Si_{0.75}$ film possess an atomic environment with Si and Ge atoms as nearest neighbour atoms. In overall terms, the EDX, GI-XRD, and Raman measurements revealed that Ge self-diffusion examined in this work on $Ge_{0.8}Si_{0.2}$ takes place inside an amorphous matrix with well dispersed Si atoms inside a Ge network.

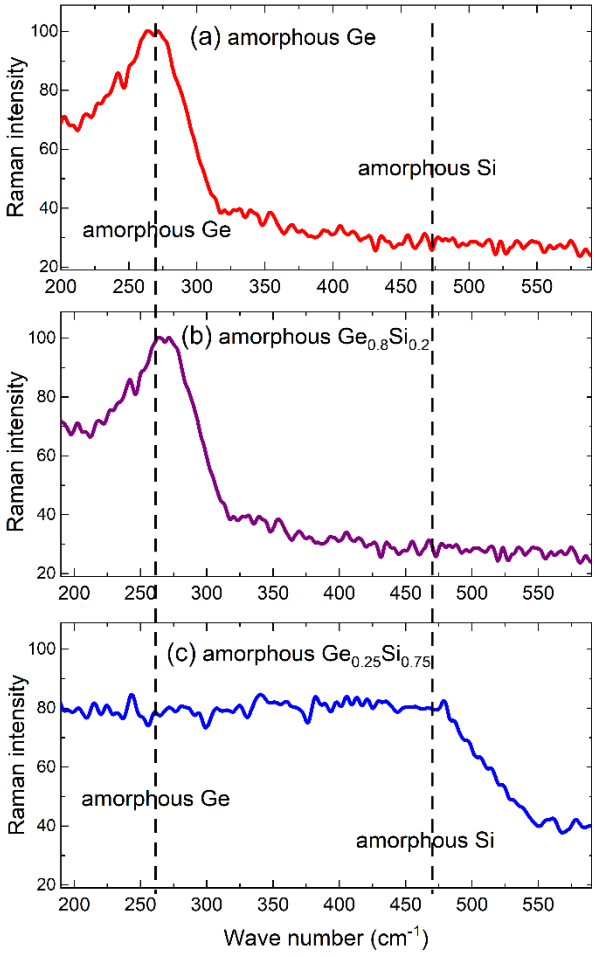

Fig. 4. Raman spectra of amorphous Ge (a), $Ge_{0.8}Si_{0.2}$ (b) and $Ge_{0.25}Si_{0.75}$ (c) films sputter-deposited on sapphire substrate.

4.2 Ge self-diffusion experiments

The Figures 5a, 6a, and 7a present three-dimensional colour maps of the in-situ measured NR data on [$^{73}Ge_{0.8}Si_{0.2}$ (14 nm) / $^{nat}Ge_{0.8}Si_{0.2}$ (14 nm)] × 10 MLs in the Rq_z^4 representation, during isothermal annealing at 397 °C, 415 °C and 436 °C, respectively. The total reflection edges are located around q_z = 0.013 Å^{-1}, and the Bragg peaks due to the Ge isotope modulation are located around q_z = 0.027 Å^{-1}. There is a Bragg peak decrease during the heat treatment. Figure 5b, 6b, and 7b plot the integrated area of the Bragg peak (termed Bragg peak intensity) of dependence on the annealing time. The integrated area is obtained by Gauss-fits to the Bragg peak. The integrated area decreases due to Ge isotope interdiffusion. Details on such experiments can be found in [6].

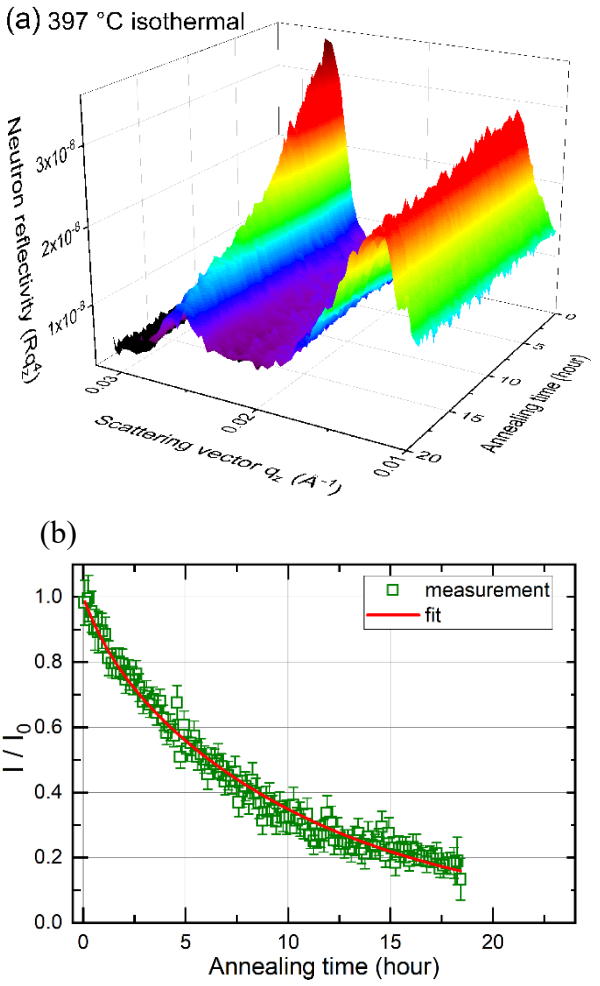

Fig. 5. In-situ measured neutron data during isothermal annealing at 397 °C of an amorphous $Ge_{0.8}Si_{0.2}$ isotope ML. a) Three dimensional color map of (Rq_z^{-4},q_z). b) Bragg peak intensity versus annealing time. The fit was performed with equation (6) with the following result $D_i = (4.0 \pm 3.5) \times 10^{-22}$ m^2s^{-1}, $D_R = (2.2 \pm 1) \times 10^{-22}$ m^2s^{-1}, and $\tau = (1.6 \pm 0.3)$ h.

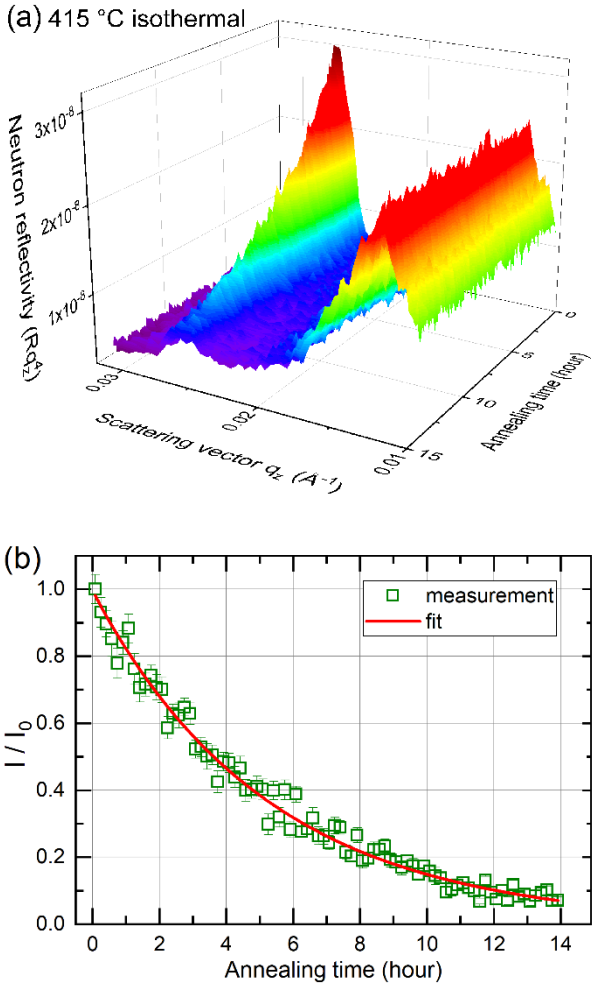

Fig. 6. In-situ measured neutron data during isothermal annealing at 415 °C of an amorphous $Ge_{0.8}Si_{0.2}$ isotope ML. a) Three dimensional color map of (Rq_z^{-4},q_z). b) Bragg peak intensity versus annealing time. The fit was performed with equation (6) with the following result $D_i = (5.5 \pm 4.5) \times 10^{-22}$ m^2s^{-1}, $D_R = (4.5 \pm 0.5) \times 10^{-22}$ m^2s^{-1}, and $\tau = (0.2 \pm 3)$ h.

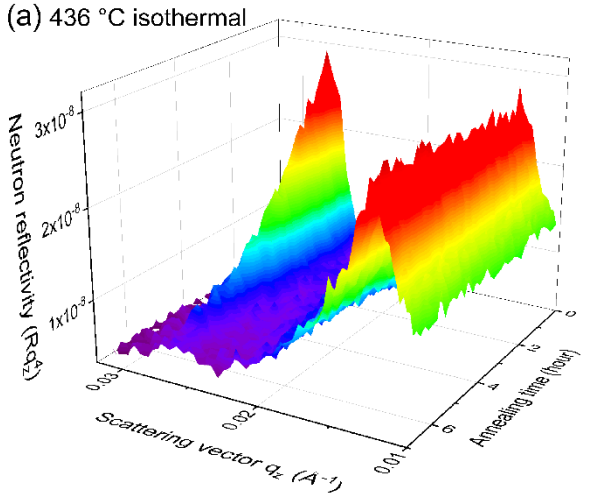

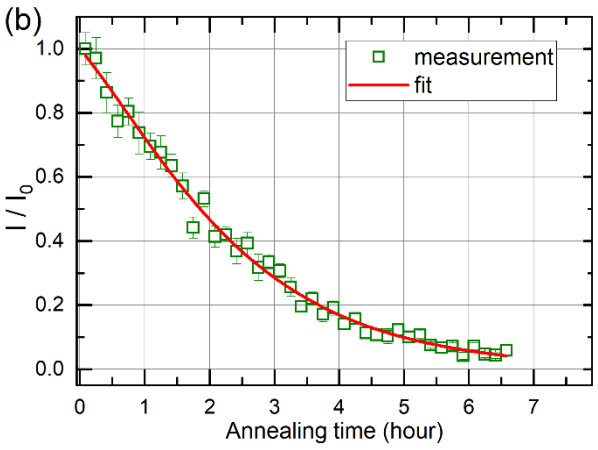

Fig. 7. In-situ measured neutron data during isothermal annealing at 436 °C of an amorphous $Ge_{0.8}Si_{0.2}$ isotope ML. a) Three dimensional color map of (Rq_z^{-4},q_z). b) Bragg peak intensity versus annealing time. The fit was performed with equation (6) with the following result $D_i = (5.5 \pm 2) \times 10^{-22}$ m^2s^{-1}, $D_R = (1.3 \pm 0.2) \times 10^{-21}$ m^2s^{-1}, and $\tau = (1.5 \pm 1)$ h.

In general, Ge self-diffusivities can be determined from the Bragg peak decrease according to the simple equation

$$D_{average} = \frac{r^2 \cdot ln\left(\frac{I_0}{I}\right)}{8 \cdot \pi^2 \cdot t} \quad , \qquad (2)$$

assuming that the diffusivity, $D_{average}$, is constant during the heat treatment. I_0 and I is the Bragg peak intensity before annealing and at the time t of the annealing process, respectively. The bilayer thickness is given by r. In case of the diffusivity changes during the annealing process, equations (3-5) have to be used instead of equation (2) [6,29]. The equations determine the average diffusivity, $D_{average}$, over the time interval t. This analysis is more appropriate for amorphous films, where the annealing process may change defects densities, e.g., frozen defects produced by the sputter-deposition process [6]. For that case, the average diffusivity for a given time interval t, is given by

$$D_{average}(t) = \frac{1}{t} \cdot \int_0^t D(t') \cdot dt' \quad , \qquad (3)$$

where $D(t)$ represents the instantaneous diffusivity at time t which can be described as

$$D(t) = D_R + (D_i - D_R) \cdot exp\left(-\frac{t}{\tau}\right) \qquad (4)$$

where D_R, D_i, and τ, are the diffusivity in the relaxed state and in the initial (t = 0) state, respectively (see references [6,29]). Integration of equation (3) (see references [6,29]) leads to the following expression

$$D_{average}(t) = D_R + (D_i - D_R)\left(\frac{\tau}{t}\right) \cdot \left(1 - exp\left(-\frac{t}{\tau}\right)\right) \qquad (5)$$

Combining relation (2) and (5) the following expression for the Bragg peak intensity decrease is obtained

$$\frac{I}{I_0} = exp\left\{-\frac{8\cdot\pi^2}{r^2}\cdot\left[D_R + (D_i - D_R)\cdot\tau\cdot\left(1 - -exp\left(-\frac{t}{\tau}\right)\right)\right]\right\} \quad . \qquad (6)$$

Equation (6) was used to fit the Bragg peak decrease in Figure 4b, 5b, and 6b, with D_R, D_i, and τ as fit variables. The obtained annealing time dependence of the instantaneous diffusivities is plotted in Figure 8. For isothermal annealing at 397 °C (Figure 8a), the diffusivity decreases by a factor of 2. This is a low decrease in instantaneous diffusivity compared to other reports on amorphous samples [6,29]. For example, the diffusivity in amorphous pure Ge films decreases by almost one order of magnitude (Figure 8b). Moreover, quite surprising, the diffusivity relaxation is almost non-existent for isothermal annealing at 415 °C (Figure 8c), and even reversed (i.e., diffusivity increases during the relaxation process) for annealing at 436 °C (Figure 8d). Noticeably, the determined instantaneous diffusivities at t = 0, are almost independent of the annealing temperature.

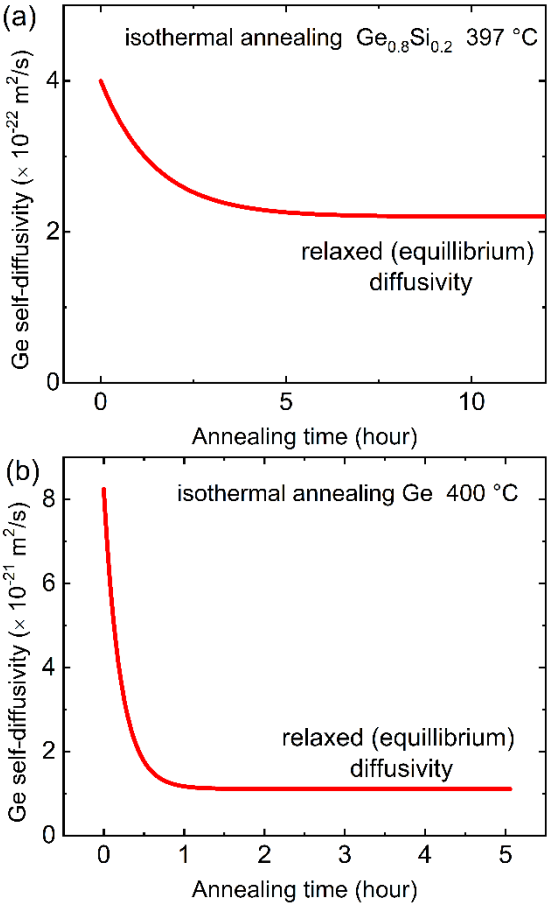

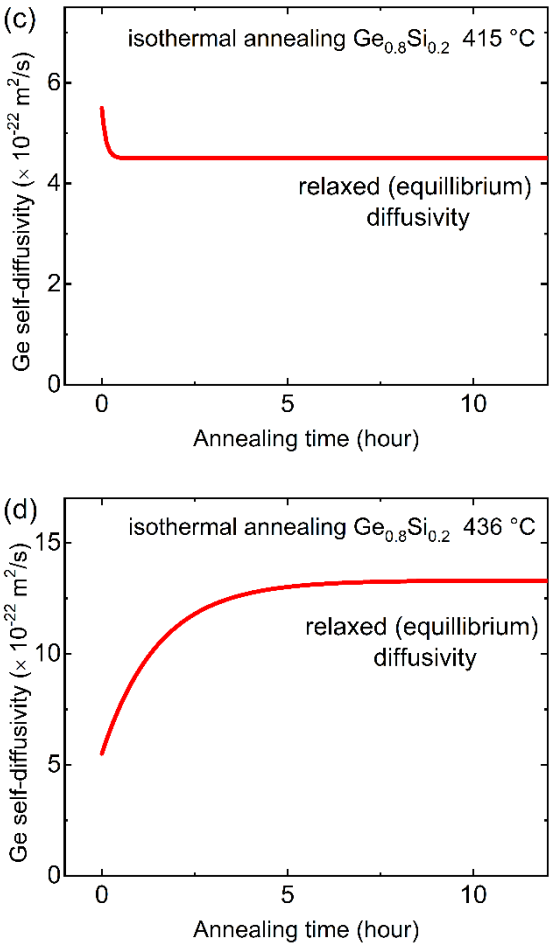

Fig. 8. Modification of the instantaneous Ge self-diffusivity in amorphous $Ge_{0.8}Si_{0.2}$ (a,c,d) and amorphous Ge (b) films as obtained by in-situ NR measurements during isothermal annealing at (a) 398 °C, (b) 400 °C, (c) 415 °C, and (c) 436 °C.

The obtained diffusivities in relaxed amorphous $Ge_{0.8}Si_{0.2}$ are plotted in Figure 9 as red filled triangles in Arrhenius representation. They obey the Arrhenius law with an activation energy of (2.06 ± 0.10) eV. For comparison, the diffusivities of relaxed amorphous Ge films are plotted as black-filled circles (with an activation energy of (2.11 ± 0.12) eV). The dotted blue line shows the Si self-diffusivities calculated from the reported activation energy of Si self-diffusion in amorphous pure silicon of (2.7 ± 0.11) eV as determined by Kirschbaum et al. [27]. The amorphous silicon was produced by Si ion-implantation and self-diffusion was investigated ex-situ after annealing the samples between 460 °C and 600 °C and cooling to room temperature afterwards. We assume that Si and Ge diffusion in amorphous $Ge_{0.8}Si_{0.8}$ is similar as also shown in Figure 1.

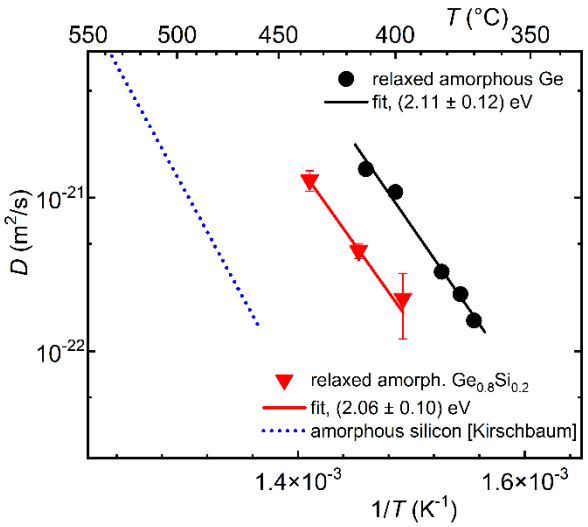

Fig. 9. Arrhenius plot of Ge self-diffusivities in relaxed amorphous $Ge_{0.8}Si_{0.2}$ films obtained during isothermal annealing and in-situ NR experiments (red triangles). Also shown are Si self-diffusivities in amorphous silicon (dotted blue line, Kirschbaum et al. [27], ion-implantation) and Ge self-diffusivities in amorphous relaxed germanium (black dots, [6], sputter deposition). Note that for sputtered amorphous silicon a higher activation energy of (4.4 ± 0.3) eV is found for temperatures above 500 °C [39].

The Ge self-diffusivities of amorphous $Ge_{0.8}Si_{0.2}$ are lower than of that of amorphous Ge by a factor of about five, while the activation energy is the same within error limits. The latter aspect indicates that the Ge self-diffusion mechanism is similar in both materials, in spite of the existence of Si-Ge bonds. The existence of Si atoms in the amorphous Ge network decreases the Ge self-diffusivities as also found for crystalline counterparts. The fact that the activation energy remains unchanged is similar to the results found for the crystalline system by Zangenberg et al. [23] and McVay et al. [13].

5 Conclusion

Literature shows that self-diffusion in crystalline silicon and crystalline germanium proceeds by different mechanisms. In crystalline germanium, literature reports self-diffusion to be mediated by single-vacancies. In contrast, self-diffusion in crystalline silicon is more complex, with contributions of self-interstitials and vacancies, but is governed predominantly by self-interstitials at high temperatures. Thus, the mixture (i.e. alloying) between germanium and silicon may cause peculiar self-diffusion. Literature also reports on self-diffusion in crystalline Ge_xSi_{1-x}, but not in the amorphous counterparts, which is presented here for the case of amorphous $Ge_{0.8}Si_{0.2}$.

The investigation of Ge self-diffusion in $Ge_{0.8}Si_{0.2}$ was performed by in-situ NR measurements during isothermal heating. All Ge self-diffusivities obtained for amorphous $Ge_{0.8}Si_{0.2}$ are smaller than that of amorphous germanium, but higher than that of amorphous silicon. The experiments revealed that the Ge self-diffusivities show a peculiar fast modification as a function of annealing time due to structural relaxation. The self-diffusivities in relaxed $Ge_{0.8}Si_{0.2}$ obey to the Arrhenius law, and have an activation energy of (2.06 ± 0.10) eV which is similar to that in relaxed amorphous germanium of (2.11 ± 0.12) eV, and different to that in amorphous silicon of (2.7 ± 0.1) [27] or (4.4 ± 0.3) [39] eV. This indicates that the Si content of 20 at.% does not change the diffusion mechanism in amorphous $Ge_{0.8}Si_{0.2}$ compared to pure Ge.

This work is based upon experiments performed at the Swiss spallation neutron source SINQ, Paul Scherrer Institut (PSI), Villigen, Switzerland. The research project has been supported by the German Research Foundation under the contract Schm1569/28–2.

References

1. Y. Shiraki, N. Usami, Edts., *Silicon–germanium (SiGe) nanostructures. Production, properties and applications in electronics*. Woodhead Publishing, Sawston, Cambridge, UK, Philadelphia, USA (2011). ISBN 978-0-85709-142-0.
2. E. Hüger, K. Osuch, *"Quantum well states in thin (110)-oriented Au films and k-space symmetry,"* Eur. Phys. J. B **37,** 149–162 (2004). https://doi.org/10.1140/epjb/e2004-00041-1.
3. M. Stutzmann, R. A. Street, C. C. Tsai, J. B. Boyce, S. E. Ready, *"Structural, optical, and spin properties of hydrogenated amorphous silicon-germanium alloys,"* J. Appl. Phys. **66**, 569-592 (1989).
4. B. Liu, L. Bai, X. Zhang, D. Zhang, C. Wei, J. Sun, Q. Huang, X. Chen, J. Ni, G. Wang, Y, Zhao, "*Light management in hydrogenated amorphous silicon germanium solar cells*," Solar Energy Materials and Solar Cells **128**, 1-10 (2014). https://doi.org/10.1016/j.solmat.2014.05.008.
5. S. Sreejith, J. Ajayan, S. Kollem, B. Sivasankari, "*A Comprehensive Review on Thin Film Amorphous Silicon Solar Cells*," Silicon **14**, 8277-8293 (2022). https://doi.org/10.1007/s12633-021-01644-w.
6. E. Hüger, F. Strauß, J. Stahn, J. Deubener, M. Bruns, and H. Schmidt, "*In-situ Measurement of Self-Atom Diffusion in Solids Using Amorphous Germanium as a Model System*," Scientific Reports **8**, 17607 (2018). https://doi.org/10.1038/s41598-018-35915-1.
7. P. Heitjans, J. Kärger, *Diffusion in condensed matter. methods, materials, models*. Springer, Berlin, Germany (2005).
8. H. Mehrer, *Diffusion in solids. Fundamentals, methods, materials, diffusion-controlled processes,* Springer, Berlin, Germany (2007).
9. E. Hüger, D. Uxa, F. Yang, and H. Schmidt, "*The Lithiation Onset of Amorphous Silicon Thin-Film Electrodes*," APL Special Topic New technologies and applications of advanced batteries, Appl. Phys.

Lett. **221**, 133901 (2022). https://doi.org/10.1063/5.0109610

10. K. Zhang, E. Hüger, Y, Li, H. Schmidt, F. Yang, "*Review and stress analysis on the lithiation onset of amorphous silicon films,"* Batteries **9**, 105 (2023). https://doi.org/10.3390/batteries9020105.
11. E. Hüger, L. Riedel, J. Zhu, J. Stahn, P. Heitjans, and H. Schmidt, "*Lithium niobate for fast cycling in Li-ion batteries: Review and new experimental data,"* Batteries **9**, 244 (2023). https://doi.org/10.3390/batteries9050244.
12. D. Uxa, E. Hüger, K. Meyer, L. Dörrer, H. Schmidt, "*Lithium-ion Diffusion in Near-stoichiometric Polycrystalline and Monocrystalline LiCoO2,"* Chem. Mater. **35**, 3307–3315 (2023). https://doi.org/10.1021/acs.chemmater.3c00359.
13. G. L. McVay and A. R. DuCharme, *"Diffusion of Ge in SiGe alloys,"* Phys. Rev. B **9**, 627-631 (1974).
14. J. Rahn, E. Hüger, L. Dörrer, B. Ruprecht, P. Heitjans, and H. Schmidt, "*A SIMS study on Li diffusion in single crystalline and amorphous LiNbO3*," Defect Diffus. Forum **323-325**, 69-74 (2012). https://doi.org/10.4028/www.scientific.net/DDF.323-325.69.
15. J. Rahn, E. Hüger, L. Dörrer, B. Ruprecht, P, Heitjans, and H. Schmidt, "*Li Self-Diffusion in Lithium Niobate Single Crystals at Low Temperatures,"* Phys. Chem. Chem. Phys. **14**, 2427 (2012). https://doi.org/10.1039/C2CP23548J
16. J. Uhlendorf, B. Ruprecht, E. Witt, C. V. Chandran, L. Dörrer, E. Hüger, F. Strauß, P. Heitjans, and H. Schmidt, "*Slow Lithium Transport in Metal Oxides on the Nanoscale*," Z. Phys. Chem. **231**, 1423–1442 (2017). https://doi.org/10.1515/zpch-2016-0939.
17. E. Hüger, L. Dörrer, and H. Schmidt, "*Permeation, Solubility, Diffusion and Segregation of Lithium in Amorphous Silicon Layers*," Chem. Mater. **30**, 3254–3264 (2018). https://doi.org/10.1021/acs.chemmater.8b00186.
18. E. Hüger, and H. Schmidt, "*Li Permeability Increase in Nano-Sized Amorphous Silicon Layers*," J. Phys. Chem. C **122**, 28528–28536 (2018).
19. J. Uhlendorf, Z. Galazka, and H. Schmidt, "*Oxygen diffusion in beta-Ga2O3 single crystals at high temperatures*," Appl. Phys. Lett. **119**, 242106 (2021). https://doi.org/10.1063/5.0071729.
20. F. Strauß, E. Hüger, J. Julin, F. Munnik, and H. Schmidt, "*Lithium Diffusion in Ion-Beam Sputter-Deposited Lithium-Silicon Layers*," J. Phys. Chem. C **124** 8616–8623 (2020). https://doi.org/10.1021/acs.jpcc.0c01244.
21. L. Dörrer, P. Tuchel, E. Hüger, R. Heller, and H. Schmidt, "*Hydrogen diffusion in proton-exchanged lithium niobate single crystals*," J. Appl. Phys. **129**, 135105 (2021). https://doi.org/10.1063/5.0047606.
22. D. Uxa, E. Hüger, K. Meyer, L. Dörrer, and H. Schmidt, "*Lithium-ion Diffusion in Near-stoichiometric Polycrystalline and Monocrystalline LiCoO2*," Chem. Mater. Submitted Manuscript ID: cm-2023-003599.R1 (2023).
23. N. R. Zangenberg, J. Lundsgaard Hansen, J. Fage-Pedersen, and A. Nylandsted Larsen, "Ge Self-Diffusion in Epitaxial Si1-xGex Layers," PRL **87**, 125901 (2001). DOI: 10.1103/PhysRevLett.87.125901
24. R. Kube, H. Bracht, J. Lundsgaard Hansen, A. Nylandsted Larsen, E. E. Haller, S. Paul, and W. Lerch, *"Composition dependence of Si and Ge diffusion in relaxed Si1−xGex alloys,"* J. Appl. Phys. **107**, 073520 (2010). https://doi.org/10.1063/1.3380853.
25. R. Kube, H. Bracht, E. Hüger, H. Schmidt, J. L. Hansen, A. N. Larsen, J. W. Ager III, E. E. Haller, T. Geue, and J. Stahn, "Contributions of vacancies and self-interstitials to self-diffusion in silicon under thermal equilibrium and nonequilibrium conditions," Phys. Rev. B **88**, 085206 (2013). https://doi.org/10.1103/PhysRevB.88.085206.
26. T. Südkamp, H. Bracht, "Self-diffusion in crystalline silicon: A single diffusion activation enthalpy down to 755 °C," Phys. Rev. B **94**, 125208 (2016). https://doi.org/10.1103/PhysRevB.94.125208.
27. J. Kirschbaum, T. Teuber, A. Donner, M. Radek, D. Bougeard, R. Böttger, J. Lundsgaard Hansen, A. Nylandsted Larsen, M. Posselt, and H. Bracht, "*Self-Diffusion in Amorphous Silicon by Local Bond Rearrangements*," PRL **120**, 225902 (2018). DOI: 10.1103/PhysRevLett.120.225902.
28. H. Schmidt, M. Gupta, and M. Bruns, "*Nitrogen diffusion in amorphous silicon nitride isotope multilayers probed by neutron reflectometry*," Phys. Rev. Lett. **96**, 055901 (2006). https://doi.org/10.1103/PhysRevLett.96.055901.
29. H. Schmidt, W. Gruber, T. Gutberlet, M. Ay, J. Stahn, U. Geckle, and M. Bruns, "*Structural relaxation and self-diffusion in covalent amorphous solids: Silicon nitride as a model system*," J. Appl. Phys. **102**, 043516 (2007). https://doi.org/10.1063/1.2770821
30. H. Schmidt, M. Gupta, J. Stahn, T. Gutberlet, and M. Bruns, "*How to Measure Self-Diffusivities in the Sub-Nanometer Range*," Acta Mater. **56**, 464-470 (2008). https://doi.org/10.1016/j.actamat.2007.10.005.
31. E. Hüger, H. Schmidt, J. Stahn, B. Braunschweig, U. Geckle, M. Bruns, "*Atomic Transport in Metastable Compounds: A Case Study on Si-C-N*," Phys. Rev. B. **80**, R220101 (2009). https://doi.org/10.1103/PhysRevB.80.220101.
32. E. Hüger, H. Schmidt, T. Geue, J. Stahn, U. Tietze, D. Lott, A. Markwitz, U. Geckle, and M. Bruns, "*Nitrogen Self-Diffusion in Magnetron Sputtered Si-C-N Films*," J. Appl. Phys. **109**, 093522 (2011). https://doi.org/10.1063/1.3585780.
33. E. Hüger, J. Rahn, J. Stahn, T. Geue, and H. Schmidt, "*Diffusivity determination in bulk*

materials on nanometric length scales," Phys. Rev. B **85**, 214102 (2012). https://doi.org/10.1103/PhysRevB.85.214102.

34. E. Hüger, J. Rahn, T. Geue, J. Stahn, P. Heitjans, and H. Schmidt, "*Lithium Diffusion in Congruent LiNbO3 Single Crystals at Low Temperatures Probed by Neutron Reflectometry*," PCCP **16**, 3670-3674 (2014). https://doi.org/10.1039/C3CP54939A.
35. S. Chakravarty, E. Hüger, H. Schmidt, J. Stahn, M. Horisberger, and N. P. Lalla, "*Self-diffusivities in Ultra-Fine Grained Metals Using Neutron Reflectometry*," Scripta Mater. **61**, 1117 (2009). https://doi.org/10.1016/j.scriptamat.2009.08.035.
36. H. Schmidt, S. Chakravarty, M. Jiang, E. Hüger, P. K. Parida, T. Geue, J. Stahn, U. Tietze, D. Lott, "*Grain Boundary Self-diffusion in Fe Films with a Stable Nanostructure*," J. Mater. Sci. **47**, 4087–4092 (2012). https://doi.org/10.1007/s10853-012-6262-0.
37. E. Hüger, R. Kube, H. Bracht, J. Stahn, T. Geue, and H. Schmidt, "*A neutron reflectometry study on silicon self-diffusion at 900 °C*," Phys. Status Solidi B **11**, 2108-2112 (2012). https://doi.org/10.1002/pssb.201248330.
38. [38=NR11] E. Hüger, U. Tietze, D. Lott, H. Bracht, E. E. Haller, D. Bougeard, and H. Schmidt, "*Self-diffusion in Germanium Isotope Multilayers at Low Temperatures*," Appl. Phys. Lett. **93**, 162104 (2008). https://doi.org/10.1063/1.3002294.
39. F. Strauß, L. Dörrer, T. Geue, J. Stahn, A. Koutsioubas, S. Mattauch, and H. Schmidt, "*Self-diffusion in amorphous silicon*," Phys. Rev. Lett. **116**, 025901 (2016). https://doi.org/10.1103/PhysRevLett.116.025901.
40. E. Hüger, J. Stahn, and H. Schmidt, "*Activation energy of diffusion determined from a single in-situ neutron reflectometry experiment*," Mat. Res. Lett. **11**, 53 (2023). https://doi.org/10.1080/21663831.2022.2114814.
41. E. Hüger, L. Dörrer, J. Rahn, T. Panzner, J. Stahn, G. Lilienkamp, and H. Schmidt, "*Lithium Transport through Nanosized Amorphous Silicon Layers*," Nano Lett. **13**, 1237–1244 (2013). https://doi.org/10.1021/nl304736t.
42. E. Hüger, J. Stahn, and H. Schmidt, "*Neutron reflectometry to measure in-situ Li permeation through ultrathin silicon layers and interfaces*," J. Electrochem. Soc. 162, A7104 (2015). DOI 10.1149/2.0131513jes.
43. E. Hüger, J. Stahn, P. Heitjans, and H. Schmidt, "*Neutron Reflectometry to Measure in-situ the Rate Determining Step of Lithium Ion Transport through Thin Silicon Layers and Interfaces*," PCCP **21**, 16444-16450 (2019). https://doi.org/10.1039/C9CP01222B.
44. F. Strauß, E. Hüger, P. Heitjans, T. Geue, J. Stahn, and H. Schmidt, "*Li Permeation through Thin Lithium-Silicon Films for Battery Applications Investigated by Neutron Reflectometry*," Energy Technol. **4**, 1582-1587 (2017). https://doi.org/10.1002/ente.201600209.
45. E. Hüger, L. Dörrer, R. Yimnirun, J. Jutimoosik, J. Stahn, and A. Paul, "Lithium permeation within lithium niobate multilayers with ultrathin chromium, silicon and carbon spacer layers," PCCP 20, 23233-23243 (2018). https://doi.org/10.1039/C8CP03345E.
46. B. Jerliu, L. Dörrer, E. Hüger, G. Borchardt, R. Steitz, U. Geckle, V. Oberst, M. Bruns, O. Schneider, and H. Schmidt, "*Neutron Reflectometry Studies on the Lithiation of Amorphous Silicon Electrodes in Lithium-Ion Batteries*," PCCP **15**, 7777-7784 (2013). DOI: 10.1039/c3cp44438d.
47. B. Jerliu, L. Dörrer, E. Hüger, B.-K. Seidlhofer, R. Steitz, U. Geckle, V. Oberst, M. Bruns, and H. Schmidt, "*Volume Expansion during Lithiation of Amorphous Silicon Thin Film Electrodes Studied by In-Operando Neutron Reflectometry*," J. Phys. Chem. C **118**, 9395–9399 (2014). https://doi.org/10.1021/jp502261t.
48. B.-K. Seidlhofer, B. Jerliu, M. Trapp, E. Hüger, S. Risse, R. Cubitt, H. Schmidt, R. Steitz, M. Ballauff, "*Lithiation of Crystalline Silicon As Analyzed by Operando Neutron Reflectivity*," ACS Nano **10**, 7458–7466 (2016). https://doi.org/10.1021/acsnano.6b02032.
49. B. Jerliu, E. Hüger, M. Horisberger, J. Stahn, and H. Schmidt, "*Irreversible lithium storage during lithiation of amorphous silicon thin film electrodes studied by in-situ neutron reflectometry*," J. Power Sources 359, 415-421 (2017). https://doi.org/10.1016/j.jpowsour.2017.05.095.
50. B. Jerliu, E. Hüger, L. Dörrer, B.-K. Seidlhofer, R. Steitz, M. Horisberger, and H. Schmidt, "*Lithium Insertion into Silicon Electrodes Studied by Cyclic Voltammetry and Operando Neutron Reflectometry*," PCCP **20**, 23480-23491 (2018). https://doi.org/10.1039/C8CP03540G.
51. D. Uxa, B. Jerilu, E. Hüger, L. Dörrer, M. Horisberger, J. Stahn, and H. Schmidt, "*On the Lithiation Mechanism of Amorphous Silicon Electrodes in Li-Ion Batteries*," J. Phys. Chem. C **123**, 22027–22039 (2019). https://doi.org/10.1021/acs.jpcc.9b06011.
52. H. Schmidt, B. Jerliu, E. Hüger, and J. Stahn, "*Volume Expansion of Amorphous Silicon Electrodes during Potentiostatic Lithiation of Li-Ion Batteries*," Electrochem. Commun. **115**, 106738 (2020). https://doi.org/10.1016/j.elecom.2020.106738.
53. Available online: http://www.ncnrs.nist.gov/resources/sldcalc.html (accessed on 22 December 2022).
54. A. Pedersen, L. Pizzagalli, H. Jonsson, "*Atomic and electronic structures of a vacancy in amorphous silicon*," Phys. Rev. B **101**, 054204 (2020). DOI: 10.1103/PhysRevB.101.054204
55. M. W. Cleveland, M. J. Demkowicz, "*Persistence of negative vacancy and self-interstitial formation*

energies in atomistic models of amorphous silicon," Phys. Rev. Mat. **6**, 013611 (2022). https://doi.org/10.1103/PhysRevMaterials.6.013611.

56. J.R. Weber, A. Janotti, C. G. Vanm de Walle, "*Dangling bonds and vacancies in germanium*," Phys. Rev. B **87**, 035203 (2013). DOI: 10.1103/PhysRevB.87.035203.
57. M. Posselt, H. Bracht, M. Ghorbani-Asl, D. Radic, "*Atomic mechanisms of self-diffusion in amorphous silicon*," AIP Advances **12**, 115325 (2022). doi: 10.1063/5.0111037.
58. E. Hüger, C. Jin, K. Meyer, D. Uxa, and F. Yang, "*Invited: Investigation of Carbon/Copper Multilayer to Examine the Influence of Copper Coating on the Li-Storage Performance of Carbon*," Energies **16**, 2740 (2023). https://doi.org/10.3390/en16062740.
59. J. Stahn, A. Glavic. "*Focusing neutron reflectometry*," Nucl. Instrum. Methods Phys. Res. Sect. A. **821**, 44–54 (2016).
60. C. Braun, Parratt32 or the reflectometry tool, HMI, Berlin, [http://www.helmholtz-berlin.de].
61. L.W. Veldhuizen, C.H.M. van der Werf, Y. Kuanga, N.J. Bakker, S.J. Yun, R.E.I. Schropp, "*Optimization of hydrogenated amorphous silicon germanium thin films and solar cells deposited by hot wire chemical vapor deposition*," Thin Solid Films **595**, 226–230 (2015). http://dx.doi.org/10.1016/j.tsf.2015.05.055.
62. A. G. Hernandez, A. E. Escobosa-Echavarría, Y. Kudriavtsev, "White luminescence emission from silicon implanted germanium," Appl. Surf. Sci. **428**, 1098–1105 (2018). https://doi.org/10.1016/j.apsusc.2017.09.234.
63. T. de Vrijer, B. Bouazzata, A. H. M. Smets, "Spectroscopic review of hydrogenated, carbonated and oxygenated group IV alloys," Vibrational Spectroscopy **121**, 103387 (2022). https://doi.org/10.1016/j.vibspec.2022.103387.